Quantitative Determination of HD Internal State Distributions via (2 + 1) REMPI*

KLAUS-DIETER RINNEN,[a] DAHV A.V. KLINER,[a] RICHARD N. ZARE[a]**
AND WINIFRED M. HUO[b]
[a]Department of Chemistry, Stanford University, Stanford, CA 94305-5080, USA
[b]NASA Ames Research Center, Moffett Field, CA 94035, USA

(*Received 7 March 1989*)

Abstract. The relationship between quantum state populations and ion signals in (2 + 1) resonance-enhanced multiphoton ionization (REMPI) detection of HD is investigated both experimentally, by measurements of hot-nozzle population distributions, and theoretically, by calculations of the two-photon E,F $^1\Sigma_g^+$–X $^1\Sigma_g^+$ transition moments. The experimental and theoretical relative rotational cross-sections are in good agreement for $v'' = 0$ and $v'' = 1$, but differ for $v'' = 2$ and for the relative vibrational cross-sections. Arguments are presented that saturation of the E,F–X transition is the main cause of these discrepancies. In spite of the presence of saturation, this calibration gives confidence in determining the relative internal state populations of HD from its (2 + 1) REMPI spectrum.

1. INTRODUCTION

The use of two-photon processes to probe forbidden transitions in molecules was first considered theoretically by Honig, Jortner and Szöke[1] and realized experimentally by Hochstrasser, Sung and Wessel.[2] With the advent of more powerful lasers, such transitions are often probed by resonance-enhanced multiphoton ionization (REMPI). The REMPI process also can be used to probe the nascent rotational and vibrational population distributions of products of a chemical reaction.[3]

Recently, it has become possible to observe the HD product in the chemical reaction $H + D_2 \rightarrow HD + D$ in a state-specific manner using either coherent anti-Stokes Raman spectroscopy (CARS)[4] or REMPI[5-8] via the HD E,F $^1\Sigma_g^+$ state in a (2 + 1) photon process (Fig. 1). There is much interest in this simplest of all neutral gas-phase reactions. Additionally, the ability to quantitate the rovibrational population distributions of HD is of importance in understanding a number of fundamental dynamical processes.

REMPI detection has intrinsically more sensitivity than CARS detection at low HD concentrations, but requires a knowledge of the relationship between ion signal and (v'', J'') population. We present here an experimental study of this relationship in which we use for calibration an effusive HD beam from a heated oven (960–1820 K). This allows us to derive correction factors as a function of the (v'', J'') quantum level for our particular experimental setup. We find that as a function of J'' the corrections are unimportant for HD($v'' = 0, J'' = 0$–13) and for HD($v'' = 1, J'' = 2$–11); however, for HD($v'' = 2, J'' = 2$–8) the measurements show that detection sensitivity smoothly increases as J'' is increased.

The correction factors can be compared to those calculated theoretically based on the line strengths for the HD E,F $^1\Sigma_g^+$ $(v', J' = J'')$–X $^1\Sigma_g^+$ (v'', J'') two-photon transitions. Experiment and theory both show that the variation of the two-photon cross-section with the rotational quantum number is modest (11% over the range studied) for $v'' = 0$ and $v'' = 1$. However, there is a discrepancy between the measured and predicted rotational correction factors for $v'' = 2$ and vibrational cross-section ratios. Possible sources for this behavior are discussed.

2. THEORETICAL TREATMENT

The first theoretical treatment of two-photon transitions was given by Goeppert-Mayer[9] based on Fermi's golden rule. More general considerations of two-photon

* Dedicated to Profs. J. Jortner and R.D. Levine, who kindly encouraged us.

** Author to whom correspondence should be addressed.

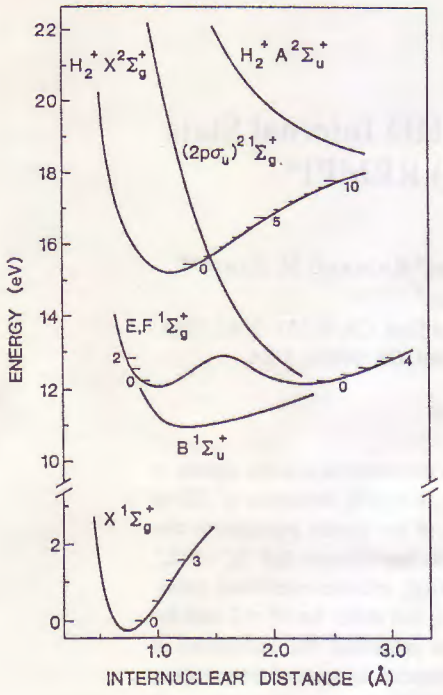

Fig. 1. Potential energy curves relevant levels to (2 + 1) REMPI of molecular hydrogen.

absorption from the viewpoint of nonlinear susceptibilities have been discussed by Butcher[10] and Bloembergen.[11] If a single frequency ω is used for pumping, the two-photon absorption rate in units of s^{-1} is given by

$$w_{f0} = (2\pi)^5 (hc)^{-2} N_0 |M_{f0}|^2 I^2 g(\omega_{f0} - 2\omega) G^{(2)}. \quad (1)$$

Here I is the single-color field intensity (in units of energy per area per second), N_0 is the Boltzmann population of the molecule in the initial state, $g(\omega_{f0} - 2\omega)$ is a normalized lineshape function, and $G^{(2)}$ is a photon statistical factor. The two-photon transition moment, M_{f0}, can be expressed as

$$M_{f0} = \sum_i \frac{\langle f | \mathbf{r}\cdot\hat{\varepsilon} | i\rangle\langle i | \mathbf{r}\cdot\hat{\varepsilon} | 0\rangle}{(E_i - E_0 - \hbar\omega)}, \quad (2)$$

where the summation is over all rovibronic states that can be coupled to the initial and final states by electric dipole-allowed transitions. The two-photon absorption cross-section is proportional to $|M_{f0}|^2$. Since the rotational quantum number of the intermediate state differs from the initial rotational quantum number by at most one in the dipole approximation, the summation over the intermediate rotational states can be carried out analytically if we assume E_i depends only on the initial rotational quantum number. For a diatomic molecule in Hund's case (a) excited by linearly polarized light, Bray and Hochstrasser[12] showed that the rotational dependence in the Q branch of a Σ–Σ transition can be expressed as

$$M_{f0} = \left(\frac{1}{9}|M_{f0}^I|^2 + \frac{4J''(J''+1)}{45(2J''-1)(2J''+3)}|M_{f0}^A|^2\right)^{1/2}. \quad (3)$$

The isotropic and anisotropic two-photon moments are

$$M_{f0}^I = M_{f0}^{\parallel} + 2M_{f0}^{\perp} \quad (4a)$$

and

$$M_{f0}^A = M_{f0}^{\parallel} - M_{f0}^{\perp}. \quad (4b)$$

The parallel component of the two-photon transition moment is given by

$$M_{f0}^{\parallel} = \sum_i \sum_{v_i} \frac{\langle \phi_f(\mathbf{r}, R)\chi_{v_f'J'}(R) | z | \phi_i(\mathbf{r}, R)\chi_{v_iJ}(R)\rangle}{E_{iv_iJ} - E_{0v_0J''} - \hbar\omega} \times \langle \phi_i(\mathbf{r}, R)\chi_{v_iJ}(R) | z | \phi_0(\mathbf{r}, R)\chi_{v_0J''}(R)\rangle, \quad (5)$$

where $\mathbf{r}$ represents the totality of electronic coordinates and R the internuclear separation. Notice that M_{f0} depends on the rotational quantum number J'' in two ways, an explicit dependence through the two-photon rotational line strength factor in Eq. (3) and an implicit dependence through the centrifugal potential used in determining the vibrational wavefunctions, $\chi_{vJ}(R)$.

Equation (5) and an analogous expression for $M_{f0}^{\perp}$ require the use of a full set of electronic and vibrational states, a computationally difficult if not impossible task. If E_i and E_0 are considered as functions of R instead of the quantum numbers v_i and J'', the summation over v_i can be carried out by closure. Equation (5) reduces to

$$M_{f0}^{\parallel}(R) = \sum_i \frac{\langle \phi_f(\mathbf{r}, R) | z | \phi_i(\mathbf{r}, R)\rangle_r}{E_i(R) - E_0(R) - \hbar\omega} \times \langle \phi_i(\mathbf{r}, R) | z | \phi_0(\mathbf{r}, R)\rangle_r \quad (6a)$$

$$M_{f0}^{\parallel} = \langle \chi_{v_f}(R) | M_{f0}^{\parallel}(R) | \chi_{v_0}(R)\rangle. \quad (6b)$$

The subscript r in Eq. (6a) denotes integration over electronic coordinates only. $M_{f0}(R)$ can be calculated using a variation-perturbation method, first applied by Honig and Jortner[13] to the calculation of multiphoton transitions and used by Moccia and Rizzo[14] to study multiphoton processes in atoms and molecules. It may also be determined by a variational dressed-state approach.[15] Physically, the neglect of explicit vibrational structure in the intermediate states can be considered as a nuclear sudden approximation where the electronic two-photon excitation occurs in a time scale

significantly faster than the relaxation of the nuclear motion. In this case, we can consider the vibrational motion to relax directly to the final state.

The present calculations of the vibrational and rotational dependence of the HD E,F $^1\Sigma_g^+$–X$^1\Sigma_g^+$ two-photon transitions followed the same procedure as described by Huo and Jaffe.[16] A composite of Eqs. (5) and (6a,b) was used. The intermediate electronic states used in the summation consisted of 53 $^1\Sigma_u^+$ and 71 $^1\Pi_u$ states. The wavefunctions for the X, the E,F, and the intermediate states were calculated at a near full-CI level using 20σ, 14π, and 6δ Slater functions. The basis set was chosen according to the rules derived by Dalgarno and Epstein[17] so that the wavefunctions satisfied the following two off-diagonal sum rules at each R:

$$S_{f0}(0) = \sum_i \{2E_i(R) - E_0(R) - E_f(R)\} \times \langle \phi_f(\mathbf{r}, R)|\mathbf{r}|\phi_i(\mathbf{r}, R)\rangle_r \times \langle \phi_i(\mathbf{r}, R)|\mathbf{r}|\phi_0(\mathbf{r}, R)\rangle_r = 0 \quad (7a)$$

and

$$S_{f0}(-1) = \sum_i \langle \phi_f(\mathbf{r}, R)|\mathbf{r}|\phi_i(\mathbf{r}, R)\rangle_r \times \langle \phi_i(\mathbf{r}, R)|\mathbf{r}|\phi_0(\mathbf{r}, R)\rangle_r = \langle \phi_f(\mathbf{r}, R)|\mathbf{r}^2|\phi_0(\mathbf{r}, R)\rangle_r. \quad (7b)$$

Since the high-lying excited states contribute more heavily to $S_{f0}(0)$ and $S_{f0}(-1)$ than to M_{f0}, we expect the convergence of the former to be a good guide to the convergence of the latter. The electronic calculations were carried out at $R = 0.8$–10.0 bohr. For the six lowest-lying electronic states, the calculations were extended to 30.0 bohr.

The number of intermediate electronic states used is too large for us to treat all vibrational structures explicitly. Previous calculations[7] showed that the four lowest-lying electronic states, B$^1\Sigma_u^+$, C$^1\Pi_u$, B$'^1\Sigma_g^+$, and D$^1\Pi_u$, were the dominant contributors to M_{f0}. Their contributions were calculated using Eq. (5), while those from the remaining 120 states were determined using Eq. (6a,b). Vibrational wavefunctions were obtained from numerical solutions of the one-dimensional Schrödinger equation, with the potential functions taken from the works of Kołos and Wolniewicz,[18,19] Wolniewicz and Dressler,[20] RKR analysis,[21] and Huo and Jaffe.[16] In the summation over v_i we included all bound and continuum levels until convergence was obtained.

We have determined the 2-photon transition moments for HD E$^1\Sigma_g^+(v' = 0, J' = J'')$–X$^1\Sigma_g^+(v'' = 0, 1, 2; J'')$, with $J'' = 0$–14 in steps of 2. The dependence of M_{f0} on the initial state vibrational quantum number is illustrated in Figs. 2 and 3. Figure 2 presents the one-photon transition moments for the B–X and E–B transitions.

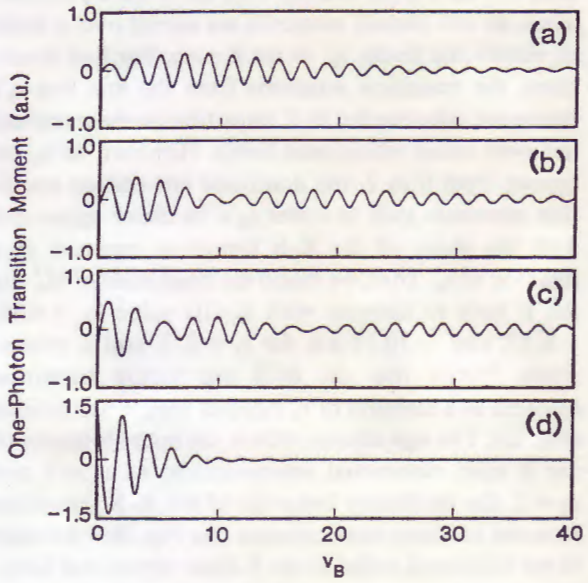

Fig. 2. One-photon transition moments for HD as a function of the vibrational quantum number v_B of the B state for the transitions B–X (v_B, 0) (a), B–X (v_B, 1) (b), B–X (v_B, 2) (c), and E–B (0, v_B) (d).

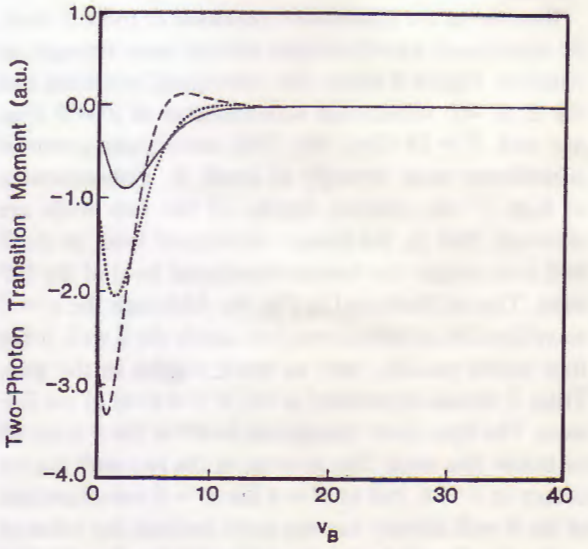

Fig. 3. Two-photon transition moment for the HD E,F–X transition as a function of the vibrational quantum number v_B of the B state. The solid line shows the two-photon transition moment for E,F–X (0, 0), the dotted line for E,F–X (0, 1), and the dashed line for E,F–X (0, 2).

Figure 3 presents $M_{f0}^{\parallel}$ determined using the $B^1\Sigma_u^+$ state alone. All moments were calculated at $J'' = 0$. The B state potential does not have good overlap with the inner well of the E,F state, and the X state potential does not have good overlap with the B state potential. Thus, all one-photon moments are spread over a range of vibrational levels, v_B, in the B state. For E–B transitions, the transition moments from the first five v_B's dominate, whereas the B–X transition moments spread out over many vibrational levels. However, as v_X increases from 0 to 2, the dominant one-photon transition moments shift to lower v_B's, in closer agreement with the shape of the E–B transition moment as a function of v_B. Thus, we found the magnitude of $M_{f0}^{\parallel}$ via the B state to increase with v_X; its value is -4.99, -8.97, and -10.19 a.u. for $v_X = 0$, 1, and 2, respectively. Notice that the B–X one-photon transition moment as a function of v_B exhibits simple oscillations (Fig. 2a). The sign change reflects the nodal behavior of the B state vibrational wavefunction. At $v_X = 1$ and $v_X = 2$, the oscillatory behavior of the B–X transition moment becomes more complex (see Fig. 2b,c) because of the additional nodes in the X-state vibrational wavefunction. In particular, the B–X transition moment for $v_X = 2$ (Fig. 2c) shows a damping that counteracts the trend of increasing overlap with the E–B transition moment. Consequently, the increase of $M_{f0}^{\parallel}$ from $v_X = 1$ to $v_X = 2$ is significantly less than from 0 to 1. Similar behavior is found in the contributions from other intermediate states.

Because of the double-well potential of the E,F state, its vibrational wavefunctions depend most strongly on rotation. Figure 4 shows the vibrational potential and the E, $v' = 0$ vibrational wavefunction at $J' = 0$ (Fig. 4a) and $J' = 14$ (Fig. 4b). The centrifugal potential contributes most strongly at small R. Consequently, at high J' the relative depths of the two wells are reversed, that is, the lowest vibrational level in the E well is no longer the lowest vibrational level of the E,F state. This is illustrated in Fig. 4b. Although the $v' = 0$ wavefunction is indeed nodeless inside the E well, it has four nodes outside, seen as weak wiggles in the plot. Thus, it should be labeled as the $v' = 4$ level of the E,F state. The first three vibrational levels of the F state all lie below this level. The reversal of the two well depths occurs at $J' = 6$, but at $J' = 4$ the $v' = 0$ wavefunction of the E well already has one node because the value of ω_e for the F well is less than that for the E well. The number of nodes increases to two at $J' = 8$ and three at $J' = 12$. Nevertheless, inside the E well the vibrational wavefunction remains nodeless and well localized.

The centrifugal potential also shifts the maximum of the E state vibrational wavefunction to larger internuclear distances. While this shift is very small, it has the effect of improving the overlap between the E state vibrational wavefunction with the four important intermediate states. Consequently, the two-photon cross-section slowly grows with J'' (Table 1). Figure 5 shows that the cross-sections are almost a linear function of $J''(J''+1)$. Note that for large J'', $B_v J''(J''+1)$

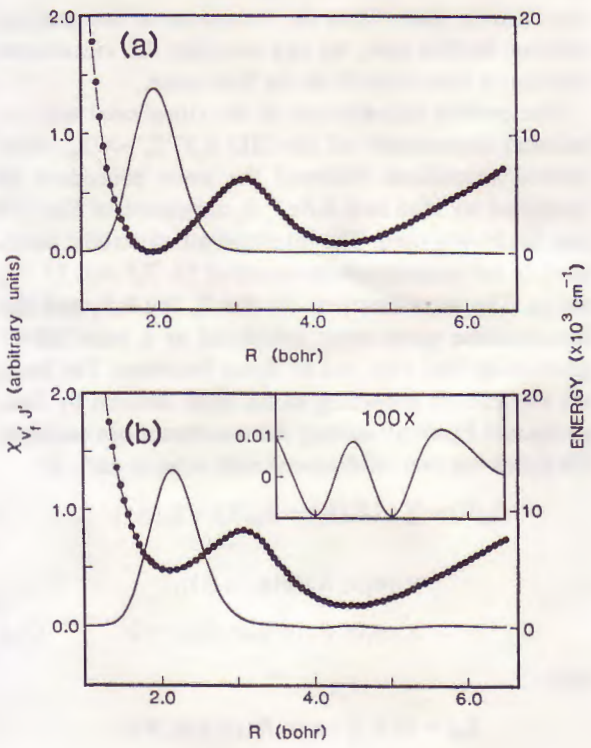

Fig. 4. Potential energy curve of the E,F well of HD (line with solid dots for calculated points) and lowest E-well vibrational wavefunction (solid line) for $J' = 0$ (a) and $J' = 14$ (b).

Table 1. Theoretical Values of $|M_{f0}|^2$ for the Transition HD E,F $^1\Sigma_g^+(v' = 0, J' = J'')$–X $^1\Sigma_g^+(v'' = 0, J'')$

	$\lvert M_{f0}\rvert^2$ (a.u.)		
J''	$v'' = 0$	$v'' = 1$	$v'' = 2$
0	6.905	22.093	28.488
2	6.940	22.244	28.730
4	7.012	22.547	29.188
6	7.127	23.029	29.916
8	7.289	23.683	30.888
10	7.453	24.465	32.172
12	7.663	25.408	33.692
14	7.956	26.587	35.469

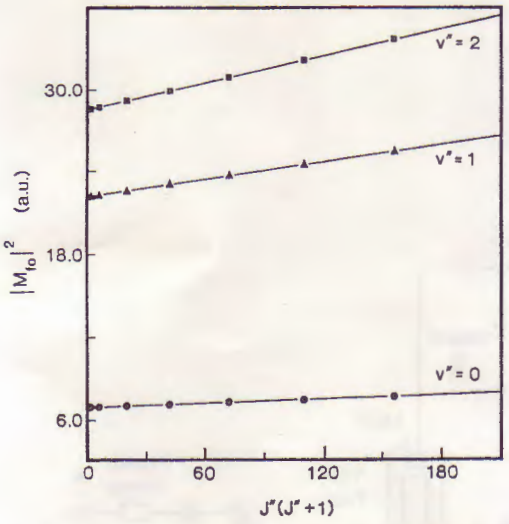

Fig. 5. Two-photon transition moment for HD E,F–X (0, v'') as a function of $J''(J''+1)$. The dots show the values for $v''=0$, the triangles for $v''=1$, and the squares for $v''=2$.

increasingly deviates from the rotational energy. The slope of $|M_{f0}|^2$ vs. $J''(J''+1)$ becomes larger as the ground state vibrational quantum number increases.

3. EXPERIMENTAL

The experimental setup (Fig. 6) is essentially identical to that described in Refs. 6–8 and therefore is only briefly discussed here. HD molecules are rotationally and vibrationally excited in a high-temperature tungsten oven. The gas effusively flows into a high-vacuum chamber and is intersected by a laser beam causing (2 + 1) REMPI. Ion detection is by time-of-flight mass spectrometry (TOF/MS).

The vacuum system consists of three differentially pumped chambers: the source chamber contains the oven, the ionization chamber is where the molecular and laser beams intersect, and the detection chamber contains the TOF/MS. The oven is mounted in the differentially pumped source chamber to avoid the introduction of a large background of rotationally and vibrationally relaxed molecules into the ionization chamber. The resistively heated tungsten oven is shown in Fig. 7. The heated part consists of a W tube (2.75 mm inner diameter, 14 cm length, 0.25 mm wall thickness), which is brazed into a copper block. A W aperture plate with an orifice size between 20 and 50 μm is electron-beam welded to the tip of the tube. For easy replacement and repair, the nozzle and mounting block are screwed into a water-cooled Cu block. A second W tube (4.7 mm inner diameter, 0.76 mm wall) is positioned concentrically to the nozzle tube and touches the nozzle tube only around the tip. Current flows from the outer to the inner tube, which has a smaller cross-section. There is no permanent joint between the tubes, but they are pressed together by a spring-loaded mechanism. This ensures good electrical contact even at elevated temperatures, at which the outer tube will stay cooler than the inner. The outer tube is directly mounted into a second water-cooled Cu block. Three Mo radiation shields isolate the outer tube from a water-cooled Cu wall (5.1 cm outer diameter). The entire oven is mounted on square stainless steel rods (1.25 cm thickness), which are attached to the top flange of the oven chamber. The top flange seals to an adjustable bellow assembly which allows the positioning of the oven with respect to the laser beam.

The nozzle temperature is measured by two thermocouples. Both are located inside the nozzle tube close to the tip. Each thermocouple is made of a W/5% Re and W/26% Re wire (Omega Engineering, Inc.). Since these materials can be used in hydrogen or inert gas atmospheres up to 2750 K, no deterioration of the wires or systematic change of the thermoelectric voltage for a given temperature is to be expected over long exposure times to the hot hydrogen atmosphere. The two pairs of thermocouple wires are insulated from each other and the oven walls by alumina (99.8% Al_2O_3) insulators. The thermoelectric voltage is converted into a temperature reading by a calibrated indicator (Omega). For any given oven temperature, the indicator readings of the two thermocouples differ by less than 3 K.

The current for the resistive heating is provided by a Variac in combination with a step-down transformer. A temperature of ~1250 K can be achieved with a current of 35 A and a voltage of 0.8 V. Since the dissipated energy is low, it is sufficient to recirculate the cooling water to the Cu mounts and shield.

The rovibrationally excited HD molecules enter the ionization chamber through a 2.5 mm diameter aperture. The distance from the oven to the aperture is ~1 cm. The laser beam intersects the gas beam ~6 cm downstream from the tip of the nozzle tube. The laser ($\lambda \sim 200$ nm) resonantly excites the HD molecules from the $X\,^1\Sigma_g^+(v'', J'')$ state to the electronically excited $E,F\,^1\Sigma_g^+(v'=0, J'=J'')$ state (Fig. 1). A third photon of the same wavelength ionizes the electronically excited molecules. The ~200 nm light is generated by frequency doubling and sum-frequency mixing (INRAD, Autotracker II) the output of a pulsed Nd:YAG-pumped dye laser (Spectra Physics, DCR 3G, PDL-1; Exciton R640/DCM, DCM) in β-barium borate (BBO) crystals.[22] The probe laser beam is focused ($f=125$ mm, planoconvex, Suprasil B) into the ionization chamber. The laser intensity is ~4 GW/cm^2 assuming a focal spot size of 100 μm and a pulse energy of 1.5 mJ.

The ions are formed between two charged, parallel plates, which extract them from the ionization region and inject them into the detection chamber containing the shuttered TOF/MS.[23] The laser power and the time-gated ion current at the CEMA detector are recorded (on each shot) as a function of laser frequency by a computer-interfaced CAMAC system.[24] "Populations" (without correction factors) are obtained by integrating the power-corrected spectral peaks (ion current divided by power squared). The power correction is considered further in the "Discussion" section.

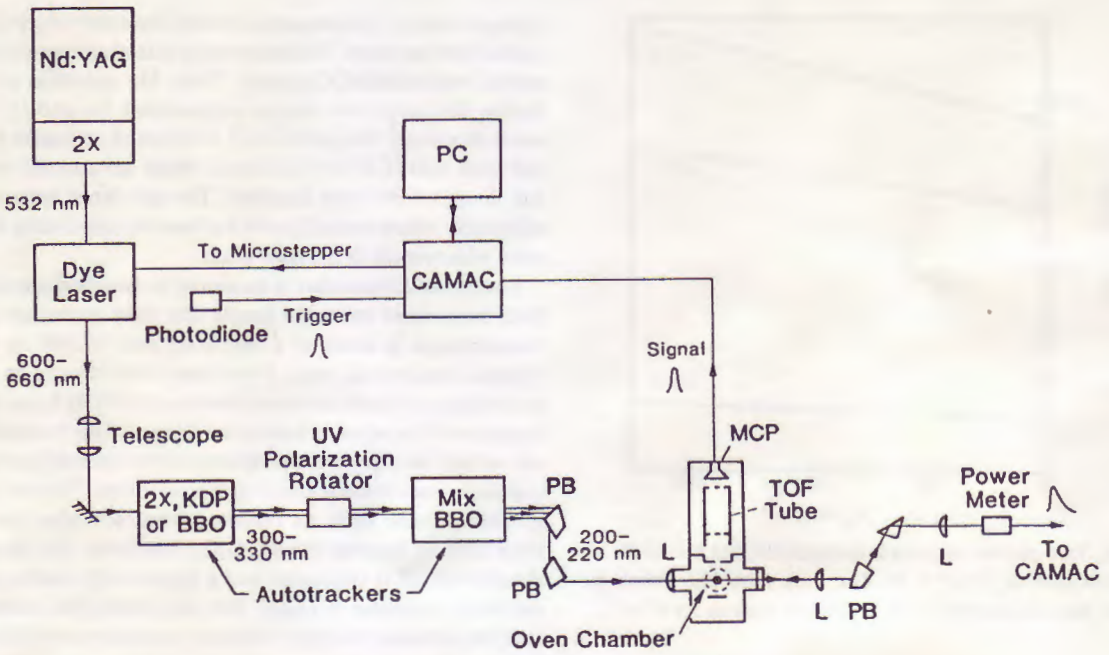

Fig. 6. Diagram of the experimental setup for oven and room temperature measurements.

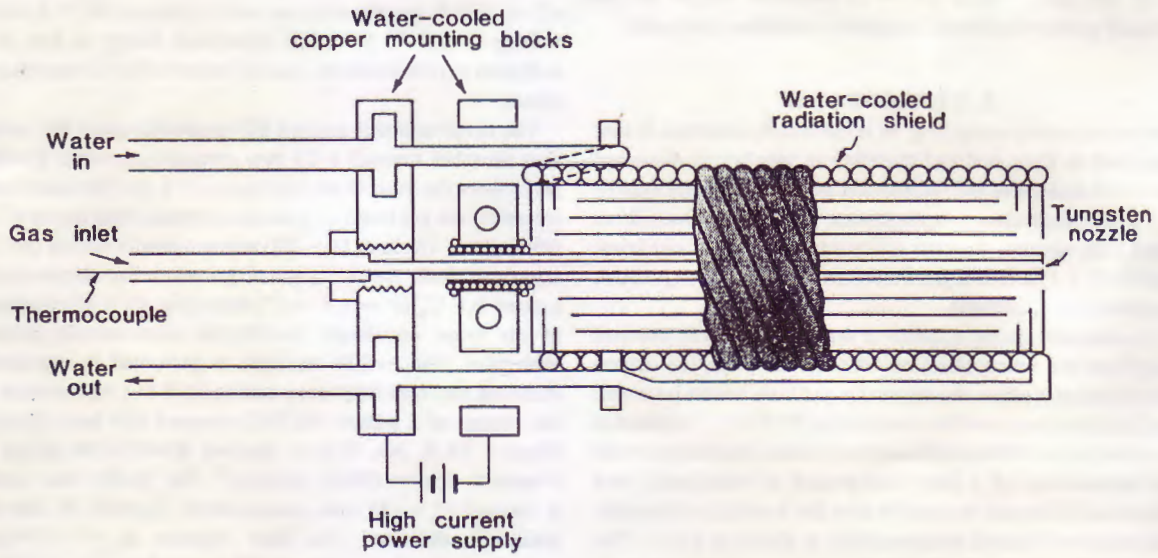

Fig. 7. Cross-sectional view of the tungsten high-temperature oven.

4. EXPERIMENTAL RESULTS

4.1. Measurements

The spectra for the levels ($v'' = 0, J'' = 0$–13), ($v'' = 1, J'' = 2$–11), and ($v'' = 2, J'' = 2$–8) of the HD ground state, X $^1\Sigma_g^+$, were recorded via Q-branch transitions through the lowest inner well vibrational level of the E,F $^1\Sigma_g^+$ state.

Oven measurements were performed with temperatures from 960 to 1820 K, pressures from 26 to 108 Torr, and orifice sizes from 20 to 50 μm. For room temperature measurements of the HD ($v'' = 0, J'' = 0$–5) levels, $\sim 2 \times 10^{-6}$ Torr of 2–5% HD in argon is bled into the ionization chamber. Any higher partial pressure of HD results in space-charge broadening of the TOF peaks and nonlinear detector response.

To generate each Boltzmann plot, the power-cor-

rected, integrated ion signals from three scans of the rotational distribution are individually normalized and averaged. A representative Boltzmann plot is given in Fig. 8. The ground state energies are calculated using the spectroscopic constants for the $X\ ^1\Sigma_g^+$ state given by Huber and Herzberg.[25] Excluding $J'' = 0, 1$ of $v'' = 0, 1$, all data points within each v'' fall on a straight line.

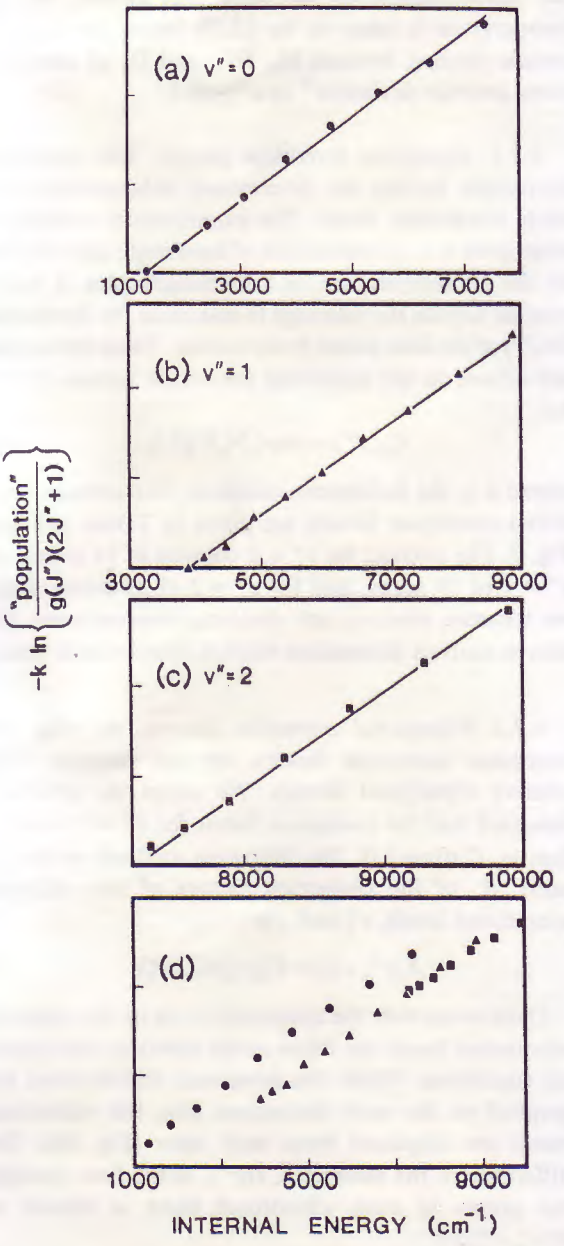

Fig. 8. Boltzmann plots for $HD(v'' = 0)$ (a), $HD(v'' = 1)$ (b), and $HD(v'' = 2)$ (c). All three vibrational bands are plotted on the same energy scale in (d). The error bars (one standard deviation) are the same size as or smaller than the symbols.

The low rotational levels ($J'' = 0$–2) are contaminated by rotationally but not vibrationally relaxed HD background gas. This background contribution could be reduced, though not eliminated, by placing a smaller aperture between the source and ionization chambers, but at the expense of signal intensity, making these measurements unreliable. Note that the internal energy of the level ($v'' = 2, J'' = 8$) is ~ 1.2 eV which is equivalent to kT at ~ 14000 K. At the highest oven temperature (1800 K), 0.02% of the HD is in ($v'' = 2, J'' = 8$). With the smaller aperture, this level could not be observed with the measured detection sensitivity of 1×10^6 molecules cm^{-3} per quantum state.

To obtain quantitative information about the relationship between ion signal and population for the (2 + 1) REMPI scheme in HD, the rovibrational population distribution of the calibration standard must be known. For oven measurements, it is necessary that the populations of all the internal states of the molecular sample can be described by a Boltzmann distribution of a given temperature. For this to hold, two experimental requirements must be fulfilled:

(a) the stagnation time of the HD molecules in the heated nozzle must be sufficiently long that the molecules can undergo sufficient collisions to equilibrate to the given temperature;

(b) the molecules cannot undergo relaxation upon issuing from the oven.

The dwell time of the molecules in the heated nozzle is estimated to be 0.5–1.0 s. Vibration-to-translation (V–T) transfer rates for HD have been measured by Barroux and Audibert[26] and Rohlfing et al.[27] Their results show that the process $HD(v = 1) + HD(v = 0) \rightarrow 2HD(v = 0)$ requires $\sim 3 \times 10^6$ hard sphere collisions (cross-section: 0.27 nm^2)[28] at room temperature and $\sim 6 \times 10^5$ collisions at 400 K (V–V transfer is faster, but does not aid in vibrational equilibration). At the temperatures accessed in the oven measurements (960–1820 K), fewer collisions would be required for V–T transfer. The $HD(v = 2)$ V–T rate is faster than that for $HD(v = 1)$, requiring $\sim 8 \times 10^5$ collisions at 298 K. Each molecule is calculated to undergo $\sim 5 \times 10^8$ collisions inside the nozzle; this is sufficient to ensure complete vibrational equilibration to the gas temperature. Rotational energy transfer rates are several orders of magnitude faster than those for V–T transfer (see following paragraph), so rotational equilibrium is also ensured. Thus, criterion (a) is satisfied.

Assuming the least favorable experimental conditions (a stagnation pressure of 110 Torr, a temperature of 1300 K, and a nozzle orifice diameter of 50 μm), the

number of hard sphere collisions within the orifice is estimated to be ~ 15. According to Kern, David and Comsa,[29] the collision number for rotational-to-translational energy transfer is ~ 200 for D_2 at a temperature of 473 K. The authors estimated the collision number for HD to be approximately one-fifth of the value for D_2. Chandler and Farrow[30] have measured rotational energy transfer rates in HD($v'' = 1$) collisions with 298 K HD gas, generating a matrix of state-to-state rotational relaxation rate constants. The fastest rate applicable to the present study, HD($v'' = 1, J'' = 2$)→ HD($v'' = 1, J'' = 1$), corresponds to a collision number of 7.6 hard sphere collisions; most rates are significantly smaller.

Because the rotational constant for HD is large (~ 45 cm^{-1}),[25] the spacing between adjacent J'' levels increases rapidly with increasing J''. Therefore, relaxation of high J'' levels proceeds more slowly than that of the low J'' levels, yielding a curved Boltzmann plot for partially relaxed HD.[31] This provides a convenient indication of the onset of rotational relaxation. Although the least favorable set of conditions may be on the border of the effusive flow regime, no relaxation (Boltzmann plot curvature) is observable below an oven pressure of ~ 200 Torr. Of course, in the absence of rotational relaxation, vibrational relaxation is negligible (see discussion above). It can be concluded that the HD is not relaxed under the present experimental conditions. Hence condition (b) is satisfied. Thus, the measured rotational distributions can be compared to Boltzmann distributions.

For each data set, a weighted linear least-squares fit of the points in the Boltzmann plot was performed. The slope of the fitted line is inversely proportional to the temperature of the gas. The measurements can be divided into two categories: room temperature and oven measurements. In the analysis of the former, the slope of the Boltzmann plot corresponds to a temperature of 290 ± 12 K (average of H_2, HD, and D_2 results[32]), in good agreement with the room temperature value of 293 K. In the oven scans, the temperature derived from the fit is found to differ from the thermocouple reading. For $v'' = 0, 1$, the temperature is found to be on average $13.7 \pm 1.5\%$ lower than the thermocouple temperature. The same average deviation was also observed for oven spectra of H_2 and $D_2(v'' = 0, 1)$.[32] There is no correlation between deviation and pressure or thermocouple temperature. This is further evidence that the molecules are not undergoing relaxation. The average deviation for $v'' = 2$ is $3 \pm 5\%$ below the thermocouple reading. The discrepancy between $v'' = 0, 1$ and $v'' = 2$ is attributed to a larger uncertainty in the $v'' = 2$ populations, and possibly to the need for rotational correction factors in $v'' = 2$.

4.2. Determination of Experimental Correction Factors

The determination of the experimental correction factors is divided into two steps: the calculation of the rotational correction factors, $C_J(J'')$, and the calculation of the vibrational correction factors, $C_v(v'')$. For the determination of the correction factors, the gas temperature is taken to be 13.7% below the thermocouple reading, because H_2, HD, and D_2 all show the same average deviation[32] in $v'' = 0, 1$.

4.2.1. Rotational correction factors. The rotational correction factors are determined independently for each vibrational band. The experimental points are compared to a calculated line of fixed slope (determined by the gas temperature) in a Boltzmann plot. A fitting routine adjusts the intercept to minimize the deviations $D(J'')$ of the data points from the line. These deviations are related to the rotational correction factors $C_J(J'')$ by:

$$C_J(J'') = \exp\{D(J'')/k\}, \tag{8}$$

where k is the Boltzmann constant. The average rotational correction factors are given in Tables 2–4 and Fig. 9. The average for $v'' = 0$ consists of 11 scans, for $v'' = 1$ of 19 scans, and for $v'' = 2$ of 22 scans. Since we measure relative, not absolute, cross-sections, the above analysis determines relative correction factors.

4.2.2. Vibrational correction factors. As with the rotational correction factors, we can measure only relative vibrational factors. We adopt the arbitrary standard that the correction factor for $v'' = 0$ is unity, that is, $C_v(0) \equiv 1.0$. The following analysis yields the ratio, R, of the correction factors of two adjacent vibrational levels, v''_a and v''_b:

$$R(v''_a, v''_b) = C_v(v''_a)/C_v(v''_b). \tag{9}$$

Oven scans over the rotational levels in two adjacent vibrational bands are taken under identical experimental conditions. When the rotational distributions are graphed on the same Boltzmann plot, the vibrational bands are displaced from each other (Fig. 8d). The difference of the intercepts, $I(v'')$, of the lines through the points in each vibrational band is related to $R(v''_a, v''_b)$ by:

$$R(v''_a, v''_b) = \exp\{[I(v''_a) - I(v''_b)]/k\}. \tag{10}$$

The intercepts $I(v'')$ are determined with the same fitting routine as used in the calculation of the rota-

Table 2. Rotational Correction Factors, $C_J(J'')$, for the Transition HD E,F $^1\Sigma_g^+(v'=0, J'=J'')$–X $^1\Sigma_g^+(v''=0, J'')$

	$C_J(J'')$	
J''	Experimental	Theoretical
0	0.93 ± 0.03	1.050
1	0.97 ± 0.02	
2	1.05 ± 0.04	1.045
3	1.00 ± 0.02	
4	0.99 ± 0.06	1.034
5	0.95 ± 0.07	
6	1.00 ± 0.09	1.017
7	1.01 ± 0.05	
8	1.00 ± 0.04	0.995
9	0.98 ± 0.05	
10	1.04 ± 0.08	0.973
11	1.07 ± 0.13	
12	1.05 ± 0.19	0.946
13	1.07 ± 0.21	
14		0.9114

Table 3. Rotational Correction Factors, $C_J(J'')$, for the Transition HD E,F $^1\Sigma_g^+(v'=0, J'=J'')$–X $^1\Sigma_g^+(v''=1, J'')$

	$C_J(J'')$	
J''	Experimental	Theoretical
0		1.042
1		
2	1.03 ± 0.06	1.035
3	1.05 ± 0.04	
4	0.94 ± 0.03	1.021
5	1.00 ± 0.08	
6	0.99 ± 0.05	1.000
7	0.98 ± 0.08	
8	0.97 ± 0.07	0.972
9	0.99 ± 0.09	
10	1.05 ± 0.13	0.941
11	1.00 ± 0.15	
12		0.906
13		
14		0.866

Table 4. Rotational Correction Factors, $C_J(J'')$, for the Transition HD E,F $^1\Sigma_g^+(v'=0, J'=J'')$–X $^1\Sigma_g^+(v''=2, J'')$

	$C_J(J'')$	
J''	Experimental	Theoretical
0		1.028
1		
2	1.14 ± 0.11	1.019
3	1.12 ± 0.10	
4	1.07 ± 0.05	1.003
5	0.98 ± 0.05	
6	0.94 ± 0.06	0.979
7	0.85 ± 0.08	
8	0.80 ± 0.12	0.948
9		
10		0.910
11		
12		0.869
13		
14		0.826

tional correction factors, i.e., the deviations of the data points from a line of fixed slope (temperature) are minimized.

Table 5 gives the relative vibrational cross-sections determined from the experimental data. The ratios $R(1, 0)$ and $R(2, 1)$ are both the average of 13 Boltzmann plots (Table 6). Note that while the rotational correction factors are multiplicative, the vibrational ones correspond to relative vibrational cross-sections. Hence, for the comparison of different vibrational bands, the measured "populations" have to be divided by the vibrational correction factors.

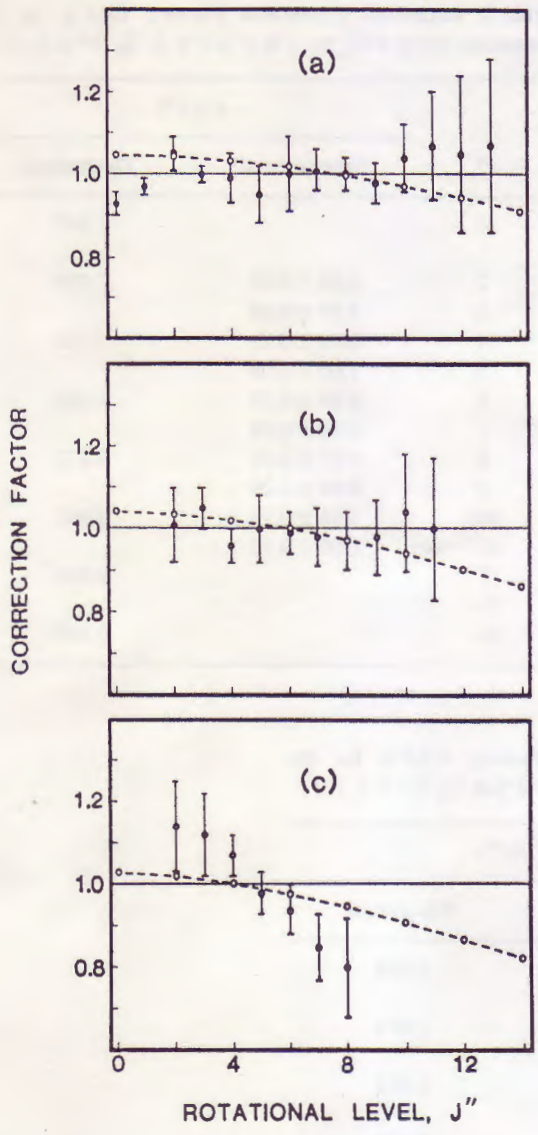

Fig. 9. Experimental (solid circles) and theoretical (open circles) rotational correction factors, $C_J(J'')$, as a function of the rotational quantum number, J'', for HD($v''=0$) (a), HD($v''=1$) (b), and HD($v''=2$) (c). Error bars represent one standard deviation. The theoretical values are connected by a broken line to guide the eye.

Table 5. Vibrational Correction Factors, $C_v(v'')$, for the Transition HD E,F $^1\Sigma_g^+(v'=0)$–X $^1\Sigma_g^+(v'')$

	$C_v(v'')$	
v''	Experimental	Theoretical
0	1.00	1.00
1	2.4 ± 0.4	3.2 ± 0.2
2	2.9 ± 0.8	4.0 ± 0.3

Table 6. Ratio R of Vibrational Correction Factors for the Transition HD E,F $^1\Sigma_g^+(v'=0)$–X $^1\Sigma_g^+(v'')$

Ratio $R(v''_a, v''_b)$	Experimental	Theoretical
$R(1,0)$	2.4 ± 0.4	3.2 ± 0.2
$R(2,1)$	1.2 ± 0.2	1.3 ± 0.1
$R(2,0)$	2.9 ± 0.4	4.0 ± 0.3

5. DISCUSSION

The measurements of the oven and room temperature spectra have allowed us to determine rotational and vibrational correction factors, so that we can relate the ion signals experimentally measured in the present apparatus to quantum state populations. The knowledge of this relationship is crucial for the accurate determination of nascent rovibrational population distributions of reactions yielding HD as a product, e.g., the $H + D_2 \rightarrow HD + D$ reaction.[5–8] The experimentally determined correction factors are independent of any theoretical description of the (2 + 1) REMPI process.

A direct comparison of the experimental correction factors with theoretical calculations of the two-photon transition moments for the bound–bound transition is possible only when the experimental conditions are such that the (v'', J'') dependence of the ion signal is free of structure resulting from the ionization step.

The power dependence of the ionization step in the (2 + 1) REMPI process is eliminated by saturating this final transition. Saturation of the ionization step was quantitatively confirmed at several representative levels of $v''=0$, 1 by using a second, time-delayed laser pulse ($\lambda = 266$ nm) to ionize the excited HD that had not been ionized by the ~200 nm pulse.[8] For strongly populated levels, ~97 ± 3% of the excited molecules are ionized by the detection laser. For less populated levels, the saturation could not be quantified, but was qualitatively confirmed.

In detecting the HD levels observed in the $H + D_2$ reaction,[5–8] the probe laser is tuned between 201 and 229 nm, corresponding to >80 nm tuning of the visible dye laser. Although power variations caused by the dye gain curve are minimized by the development of dye mixes that have relatively flat gain over the spectral region of interest, they cannot be eliminated. Thus, the observed ion signal must be power corrected. As

mentioned in the "Experimental" section, a quadratic power correction is used, reflecting the dependence of the two-photon absorption rate on laser intensity (see Eq. (1)). The saturation of the ionization step is a necessary condition for the use of such a power correction. However, Eq. (1) is strictly valid only in the limit that the two-photon transition is not saturated. At high laser intensities, saturation of the two-photon transition will occur, and the power dependence of the ion signal will be less than quadratic. For the present experimental setup, the integrated ion signal is measured to be proportional to the laser pulse energy raised to the 1.3 ± 0.2 power in $v'' = 0$ and $v'' = 1$, indicating that saturation is present. Although this is of no consequence for the calibration of the present apparatus, it does affect the comparison with the theoretical two-photon transition moments. A more complete treatment of saturation is deferred until the discussion of the comparison of experiment and theory.

Because the dependence of the ion signal on the ionization step has been minimized, a comparison is possible with the theoretical calculation of the cross-sections for the two-photon excitation step.

5.1. Rotational Correction Factors

Figure 9 compares the experimental and theoretical results. The data sets are listed in Tables 2–4. To calculate the theoretical rotational correction factors from the two-photon cross-sections, the data are inverted and rescaled to the sum of the J'' levels common with the experimental distribution.

For $v'' = 0$ and $v'' = 1$, the theoretical values agree well with the experimental data within the uncertainties. Theory predicts a slow increase of the two-photon cross-section by $\sim 11\%$ for $v'' = 0$ and $v'' = 1$ as J'' increases over the experimental range. This results in a decrease of $C_J(J'')$ by $\sim 13\%$ for $v'' = 0$ (Fig. 9a) and $\sim 14\%$ for $v'' = 1$ (Fig. 9b). The experimental data do not exhibit such a trend and scatter instead around unity. This is caused by the assumption that the correct gas temperature is 13.7% below the thermocouple reading (based on the average of the temperature deviations of the fits of $v'' = 0$ and $v'' = 1$). Since the measured temperatures of $v'' = 0$ and $v'' = 1$ are assumed to be identical to the gas temperature, a small change of the correction factors with J'' cannot be observed. A correction of the experimental data with the theoretical two-photon cross-sections results in a change of the temperature by only $\sim 2\%$, which is within the experimental uncertainty.

For $v'' = 2$, experiment and theory do not agree well (Fig. 9c). The trend of the theoretical correction factors persists, but is weaker. The decrease is $\sim 8\%$ from $J'' = 0$ to $J'' = 8$. However, the experimental values no longer scatter around unity but decrease by $\sim 30\%$. Note that there is a change of the average temperature deviation below the thermocouple reading from 13.7% for $v'' = 0$, 1 to 3% for $v'' = 2$.

To explain the observed trends, three processes are considered: the production of H^+/D^+ and the excitation of autoionizing Rydberg states are shown to be unimportant for the present detection scheme, whereas the decrease of the rotational correction factors in $v'' = 2$ may be attributed to saturation of the two-photon E,F–X transition.

5.1.1. H^+/D^+ *production*. Buck, Parker and Chandler[33] have shown that H^+ production in (2 + 1) REMPI proceeds by dissociative ionization from the $H_2^+\ ^2\Sigma_u^+$ state at internuclear distances greater than ~ 2.0 Å. It follows that only HD transitions via vibrational levels that have significant F-well character can contribute to H^+/D^+ production.

In the present study, the REMPI detection scheme proceeds exclusively through the lowest vibrational state of the E well; hence, no significant H^+/D^+ production is expected for low rotational excitation. However, for high J', the vibrational wavefunction tunnels through the barrier into the F well (Fig. 4b), adding F-well character to the vibrational wavefunction. Because the change of the amplitude of the wavefunction in the F well as a function of J' is small, this process could cause a minor increase of $C_J(J'')$ with J'', as observed for $J'' = 10$–13 of $v'' = 0$ (Fig. 9a). Note that this trend is well within the experimental uncertainties. For $v'' = 1$, no such trend is seen, but only levels up to $J'' = 11$ are recorded (Fig. 9b). The discrepancy between the theoretical and experimental results for $v'' = 2$ cannot be explained by H^+/D^+ production, since $C_J(J'')$ decreases with J'' (Fig. 9c).

5.1.2. Excitation of autoionizing Rydberg states. Xu, Helm and Kachru[34] have shown that rotational-state-selective photoionization spectra of H_2 from the E,F $^1\Sigma_g^+(v' = 0$–$2)$ state exhibit sharp resonance-like structures, which are correlated with the excitation of Rydberg states in the np series. These states decay rapidly by ejecting an electron, causing an increase in the ionization probability. This process is strongly dependent on the wavelength of the ionization laser.

In the context of the present study, autoionizing states would cause significant variations of the ionization probability as the wavelength of the detection laser is tuned. If this mechanism were important, the rota-

tional correction factors would show rapid changes as a function of J''. However, no abrupt fluctuations in $C_J(J'')$ are observed. For the wavelengths used in the experiment, the total energy is ~ 150000 cm^{-1}, substantially above the energy of the Rydberg series converging to the $HD^+X^2\Sigma_g^+$ ion state. There exists another series converging to the $HD^+A^2\Sigma_u^+$ ion state, but the shapes of the potential curves of the E,F and the Rydberg states are very different. The unfavorable Franck–Condon overlap makes autoionization through this Rydberg series unlikely.

Although the ionization step is saturated, the resonant excitation of Rydberg states cannot necessarily be neglected. As known from dissociative recombination studies,[35-37] the potential energy curves of the Rydberg states can cross with the curves of the doubly excited states leading to H(1s) + H(nl) formation. This pathway will compete with autoionization and would be experimentally manifested as fluctuations in $C_J(J'')$. As mentioned, no such fluctuations are observed. The lack of structure in $C_J(J'')$ is a fortuitous consequence of the fact that the total energy region accessed in the REMPI detection scheme lies between two Rydberg series. Hence, neither series interferes with direct ionization.

5.1.3. Saturation effects in the two-photon E,F–X *transition.* The advent of BBO permits the generation of tunable 200-nm radiation with high efficiency. The average pulse energy in this experiment is 1.5 mJ. The beam is tightly focused (~ 100 μm spot size) and the laser intensity is ~ 4 GW/cm^2 for a laser pulse duration, τ_p, of 5 ns. The frequency-integrated excitation cross-section for HD($v'' = 2, J'' = 4$) is $\sim 1.3 \times 10^{-35}$ cm^4 corresponding to a two-photon absorption cross-section of $\sim 9 \times 10^{-47}$ cm^4 s at 1400 K. A rough estimate of the criterion for saturation,[38] $w_{f0}\tau_p$, gives 9.0. Therefore, saturation of the two-photon transition occurs under our experimental conditions in accordance with the measured power dependence of the ion signal. The theoretical maximum value of $w_{f0}\tau_p$ is 1/2, which is exceeded in the above estimate because neither dephasing effects nor the change of the linewidth caused by the high laser intensity are considered. When the two-photon transition is saturated, the measured ion signals cannot be directly compared to theoretical cross-sections unless the degree of saturation is constant for all levels. This alters the experimental correction factors relative to the theoretical values. To address this problem, a complete density matrix analysis is required.

The saturation criterion depends on two parameters: the photon flux and the two-photon transition moment. The theoretical cross-sections change slowly with J'' (by $< 11\%$ for $v'' = 0, 1$ and by $\sim 8\%$ for $v'' = 2$). If the photon flux is constant within a vibrational band, the degree of saturation will be approximately constant. This is the case for $v'' = 0$ and $v'' = 1$, in which the detection laser intensity changes by $< 10\%$ while tuning over the J'' range. Therefore, the experimental and theoretical values of $C_J(J'')$ for $v'' = 0$ and $v'' = 1$ can be directly compared (Fig. 9a,b) and are independent of the degree of saturation. However, for $v'' = 2$ the laser intensity decreases by $\sim 30\%$ from $J'' = 0$ to $J'' = 8$, varying the degree of saturation by a factor of ~ 2. Hence, the detection sensitivity is diminished at low J''. This change manifests itself in a steady decrease in the magnitude of the rotational correction factors from $J'' = 2$ (1.14 ± 0.11) to $J'' = 8$ (0.80 ± 0.12) (Fig. 9c). The change in the detection sensitivity also causes a higher temperature in the Boltzmann fit to the $v'' = 2$ data. If the measured laser-power dependence of the ion signal is included in the correction factors, the discrepancy with theory is quantitatively resolved.[32] Thus, it has been experimentally verified that saturation of the bound–bound transition is the cause of the apparent discrepancy between experiment and theory in the $v'' = 2$ rotational correction factors.

5.2. Vibrational Correction Factors

Tables 5 and 6 give the experimental and theoretical values of the relative vibrational cross-sections and their ratios. The data are normalized such that $C_v(0)$ is unity in each set. The theoretical ratios are based on the average rotational two-photon cross-sections for the range of J'' studied. It is valid to determine an average $C_v(v'')$ because the dependence of the correction factors on v'' is much stronger than on J''. The experimental and theoretical results disagree outside the combined error bars, except for the ratio $R(2, 1)$.

To account for the discrepancies, several mechanisms are considered that either compete with the ionization step or affect the two-photon resonant excitation cross-section. The following processes are discussed below and rejected: radiative decay, collisional activation, H^+/D^+ production, and contribution from doubly excited states. The disagreement between the experimental and theoretical vibrational correction factors again appears to result from saturation of the two-photon transition.

5.2.1. Radiative decay. The radiative lifetime of the E,F state was measured by Kligler and Rhodes[39] to be 100 ± 20 ns. For a laser pulse length of 5 ns, at most 5% of the population in this electronically excited state is

lost by radiative decay. Because the ionization step is saturated, photoionization is the fastest loss mechanism.

5.2.2. Collisional deactivation. The $\sim 10^{-6}$ Torr pressure of HD in the interaction region with the detection laser corresponds to an average time between hard sphere collisions of ~ 40 μs at 1500 K. Collisional deactivation is negligible because ionization depletes the population of the excited level within 5 ns of excitation.

5.2.3. H^+/D^+ production. H^+/D^+ production depends solely on the character of the vibrational wavefunction of the E,F state. Because (2 + 1) REMPI detection always accesses the lowest vibrational level in the E well, the difference in $C_v(v'')$ between experiment and theory cannot be readily explained by this mechanism.

5.2.4. Contribution from doubly excited states. Superexcited states may be accessed from the E,F well either by direct photon absorption or via low energy electron recapture. For the direct one-photon excitation process, selection rules require that the repulsive state must have ungerade symmetry. In the energy region of 18 eV above the ground state of HD, the only accessible state is the $^1\Sigma_g^+$ state.[40] Because the transition to this state is forbidden, photodissociation is irrelevant to the present study.

In dissociative recombination, neutral molecules (or atoms) are produced by the recombination of molecular ions with electrons.[35–37] Since the electron recapture process follows HD^+ ion formation, it is a secondary process and must be considered only if a strong source of low-energy electrons exists. The ionization of HD is the only source of electrons ($E \sim 3$ eV) as evidenced by the dominance of the HD^+ peak in the TOF spectrum. The small cross-section ($\sim 10^{-17}$ cm^2 at $E \sim 3.0$ eV)[36,37] and low HD^+ and e^- densities make electron recapture negligible as a loss mechanism in this experiment.

5.2.5. Saturation effects in the two-photon E,F–X *transition.* The criterion for saturation,[38] $w_{fi}\tau_p$, may be estimated for each v'', as was done for $v'' = 2$ in part (5.1.3) above. The frequency-integrated excitation cross-section for $HD(v'' = 0)$ is $\sim 4 \times 10^{-36}$ cm^4, corresponding to a two-photon absorption cross-section of $\sim 3 \times 10^{-47}$ cm^4 s at 1400 K. The criterion for saturation is ~ 2.2 for $v'' = 0$. For $v'' = 1$ and $v'' = 2$, the values of $w_{fi}\tau_p$ are ~ 7.3 and ~ 9.0, respectively. Saturation of the two-photon transition occurs under our experimental conditions for all vibrational levels. This was confirmed in measurements of the power dependence of the ion signals.

Because the theoretical cross-section increases with v'' (Table 5), saturation will be most severe for transitions from excited vibrational states. The two-photon cross-sections from $v'' = 1$ and $v'' = 2$ differ by $\sim 30\%$, so both transitions are approximately equally saturated. The theoretical ratio $R(2, 1)$ is 1.3, in good agreement with experiment. However, because the theoretical value of $R(1, 0)$ is 3.2, saturation is expected to be much stronger for $v'' = 1$ than for $v'' = 0$. The experimental ratio of 2.4 mirrors the enhanced saturation of $v'' = 1$.

Saturation of the two-photon transition explains the discrepancy between theory and experiment for the relative vibrational cross-sections. A further test of the theoretical $C_v(v'')$ values would require experimental conditions in which the two-photon transition is not saturated.[32] However, saturation of the ionization step necessitates high laser intensities, complicating such a study.

5.3. Summary

The relationship between ion signal and quantum state population has been quantitatively determined for (2 + 1) REMPI detection of HD. The rotational correction factors agree well with theoretical calculations, except for $v'' = 2$. The experimental vibrational correction factors differ from the theoretical values. These discrepancies are attributed to saturation of the two-photon E,F–X transition. The saturation effect can be neglected for the rotational correction factors of $v'' = 0$ and $v'' = 1$ because the two-photon cross-section and the detection laser intensity change slowly as functions of J''. Therefore, the degree of saturation is approximately constant within these vibrational levels. The saturation of the bound–bound transition is of importance in comparing theory and experiment, but is of no consequence for the calibration of the present apparatus.

Acknowledgments. We are grateful to M. Gutierrez for his skillful assistance in the construction of the oven and to A.C. Kummel and G.O. Sitz for many useful discussions about the design. The helpful assistance of M.A. Buntine is acknowledged. We thank Y.T. Lee and B. Continetti for the HD gas used in this experiment. Graduate fellowships are gratefully acknowledged by K.-D.R. (Deutscher Akademischer Austauschsdienst, Jahresstipendium 1984/5; Rotary Foundation, 1985/6) and D.A.V.K. (National Science Foundation, 1986–89). This project is suported by the National Science Foundation under Grant No. NSF CHE 87–05131.

REFERENCES

(1) Honig, B.; Jortner, J.; Szöke, A. *J. Chem. Phys.*, 1967, **46**: 714.

(2) (a) Hochstrasser, R.M.; Sung, H.N.; Wessel, J.E. *J. Chem. Phys.*, 1974, **60**: 317. (b) Bray, R.G.; Hochstrasser, R.M.; Wessel, J.E. *Chem. Phys. Lett.*, 1974, **27**: 167.

(3) Levine, R.D.; Bernstein, R.B. *Molecular Reaction Dynamics and Chemical Reactivity*; Oxford University Press: New York, 1987.

(4) (a) Gerrity, D.P.; Valentini, J.J. *J. Chem. Phys.*, 1983, **79**: 5202; *J. Chem. Phys.*, 1984, **81**: 1298; *J. Chem. Phys.*, 1985, **82**: 1323. (b) Valentini, J.J.; Gerrity, D.P. *Int. J. Chem. Kinet.*, 1986, **18**: 937.

(5) (a) Rettner, C.T.; Marinero, E.E.; Zare, R.N. In *Physics of Electronic and Atomic Collisions*. Invited Papers from the XVIIIth ICPEAC, Berlin, July 27–August 2, 1983; Eichler, J.; Hertel, I.V.; Stolterfoht, N., Eds.; North Holland: Amsterdam, 1984; p. 51. (b) Marinero, E.E.; Rettner, C.T.; Zare, R.N. *J. Chem. Phys.*, 1984, **80**: 4141.

(6) Blake, R.S.; Rinnen, K.-D.; Kliner, D.A.V.; Zare, R.N. *Chem. Phys. Lett.*, 1988, **153**: 365.

(7) Rinnen, K.-D.; Kliner, D.A.V.; Blake, R.S.; Zare, R.N. *Chem. Phys. Lett.*, 1988, **153**: 371.

(8) Rinnen, K.-D.; Kliner, D.A.V.; Zare, R.N. *J. Chem. Phys.*; to be published.

(9) Goeppert-Mayer, M. *Ann. Phys.*, 1933, **9**: 273.

(10) Butcher, P.N. *Non-linear Optical Phenomena*; Ohio State University Engineering Publications: Columbus, 1965.

(11) Bloembergen, N. *Non-linear Optics*; Benjamin: New York, 1965.

(12) Bray, R.G.; Hochstrasser, R.M. *Mol. Phys.*, 1976, **31**: 1199. Note that the rotational line strength factor in Eq. (3) contains a factor $(2J'' + 1)^{-1}$ from averaging the initial state degeneracy.

(13) Honig, B.; Jortner, J. *J. Chem. Phys.*, 1967, **47**: 3698.

(14) Moccia, R.; Rizzo, A. *J. Phys. B*, 1985, **18**: 3319.

(15) Huo, W.M. *J. Chem. Phys.*, 1984, **81**: 3407.

(16) Huo, W.M.; Jaffe, R.L. *Chem. Phys. Lett.*, 1983, **101**: 463.

(17) Dalgarno, A.; Epstein, S.T. *J. Chem. Phys.*, 1969, **50**: 2837.

(18) Kołos, K.; Wolniewicz, L. *J. Chem. Phys.*, 1965, **43**: 2429.

(19) Kołos, K.; Wolniewicz, L. *J. Chem. Phys.*, 1968, **48**: 3672.

(20) Wolniewicz, L.; Dressler, K. *J. Mol. Spectrosc.*, 1977, **67**: 416.

(21) Sharp, T.E. *At. Data*, 1971, **2**: 119.

(22) The barium borate crystals were supplied by R.S. Feigelson and R.K. Route and grown as part of a research program sponsored in part by the Army Research Office, contract DAAL03-86-K-0129, and in part by the NSF/MRL Program through the Center for Materials Research, Stanford University.

(23) Rinnen, K.-D.; Kliner, D.A.V.; Blake, R.S.; Zare, R.N. *Rev. Sci. Instrum.*, 1989, **60**: 717.

(24) Blake, R.S. Ph.D. Dissertation; Department of Chemistry, Stanford University: Stanford, 1988.

(25) Huber, K.P.; Herzberg, G. *Molecular Spectra and Molecular Structure. IV. Constants of Diatomic Molecules*: Van Nostrand–Reinhold: New York, 1979.

(26) Barroux, C.; Audibert, M.M. *Chem. Phys. Lett.*, 1979, **66**: 483.

(27) Rohlfing, E.A.; Rabitz, H.; Gelfand, J.; Miles, R.B. *J. Chem. Phys.*, 1984, **81**: 820.

(28) Atkins, P.W. *Physical Chemistry*; W. H. Freeman and Co.: San Francisco, 1982; p. 815.

(29) Kern, K.; David, R.; Comsa, G. *J. Chem. Phys.*, 1985, **82**: 5673.

(30) Chandler, D.W.; Farrow, R.L. *J. Chem. Phys.*, 1986, **85**: 810.

(31) Pollard, J.E.; Trevor, D.J.; Lee, Y.T.; Shirley, D.A. *J. Chem. Phys.*, 1982, **77**: 4818.

(32) Rinnen, K.-D.; Kliner, D.A.V.; Buntine, M.A.; Zare, R.N.; Huo, W. M. *J. Chem. Phys.*; to be submitted.

(33) Buck, J.D.; Parker, D.H.; Chandler, D.W. *J. Phys. Chem.*, 1988, **92**: 3701.

(34) Xu, E.Y.; Helm, H.; Kachru, R. *Phys. Rev. A*, 1989, **39**: 3979 .

(35) Peart, B.; Dolder, K.T. *J. Phys. B*, 1975, **8**: 1570.

(36) Nakashima, K.; Takagi, H.; Nakamura, H. *J. Chem. Phys.*, 1987, **86**: 726.

(37) Hus, H.; Yousif, F.; Noren, C.; Sen, A.; Mitchell, J.B.A. *Phys. Rev. Lett.*, 1988, **60**: 1006.

(38) Hanna, D.C.; Yuratich, M.A.; Cotter, D. *Nonlinear Optics of Free Atoms and Molecules*; Springer-Verlag: New York, 1979; p. 174.

(39) Kligler, D.J.; Rhodes, C.K. *Phys. Rev. Lett.*, 1978, **40**: 309.

(40) Guberman, S.L. *J. Chem. Phys.*, 1983, **78**: 1404.